Anisotropic magnetic relaxation, hysteresis, and Meissner fraction in untwinned single-crystal $YBa_2Cu_3O_{7-\delta}$ produced without applying stress

J. P. Rice, D. M. Ginsberg, and M. W. Rabin
Department of Physics and Materials Research Laboratory, University of Illinois at Urbana-Champaign, 1110 West Green Street, Urbana, Illinois 61801

K. G. Vandervoort,* G. W. Crabtree, and H. Claus*
Materials Science Division, Argonne National Laboratory, Argonne, Illinois 60439
(Received 25 September 1989)

By quenching the tetragonal phase during crystal growth of $YBa_2Cu_3O_{7-\delta}$ and then oxygenating the crystals without mechanical stress, we obtain some essentially untwinned crystals. Magnetic measurements on such crystals, with fields applied along the *a* or *b* axis, show anisotropy. A qualitative analysis of our relaxation and hysteresis data indicates that the critical current density is higher along *a* than along *b* (the chain direction). The anisotropic Meissner percent data show that pinning is higher for fields along *b* than along *a*.

I. INTRODUCTION

Is there any anisotropy in the superconducting properties of $YBa_2Cu_3O_{7-\delta}$ between the *a* and *b* directions? What role do the (110) twinning planes play in determining the properties? These questions have been difficult to answer since the discovery of this high-temperature superconductor because $YBa_2Cu_3O_{7-\delta}$ crystals without significant (110) twinning were unavailable. Recently we have developed a procedure of producing some untwinned, stress-free crystals. There are two reasons for finding a way of producing untwinned crystals without subjecting them to stress. First, there is always a possibility that the application of stress will introduce dislocations or other structural defects. Second, some crystals are too thin to withstand the required stress; thin crystals are especially desirable, since one can oxidize them uniformly in a reasonably short time. In this paper we describe our preparation procedure, and present magnetic measurements on three untwinned single crystals of $YBa_2Cu_3O_{7-\delta}$ having sharp superconducting transitions near 90 K. Since our crystals are untwinned, we are able to report measurements with the magnetic field applied along all three crystal axes, determining whether there is any anisotropy between the effects obtained with *H* along the *b* axis (the Cu-O chain direction) and along the *a* axis (perpendicular to the Cu-O chain direction). One previous study compared an untwinned crystal to twinned crystals, but did not report any measurements for *H* applied along *a* or *b*.[1]

The magnetic properties of high-temperature superconductors exhibit some interesting and novel features below T_c.[2] One of these is the ease with which fluxons (quantized fluxoids) can be made to move. This feature, caused by the relatively high temperatures and low pinning energies, manifests itself in many ways, including easily observable decay of the magnetization with time.[2-5] This magnetic relaxation is important because it shows that high-temperature superconductors may not be able to support persistent currents indefinitely. Another related property is the field dependence of the Meissner fraction,[6] which can serve as a probe of the pinning energies. It has been suggested that pinning is an intrinsic property of the crystal lattice because of the short coherence lengths in these superconductors.[7,8] Thus, the pinning might be expected to be anisotropic in the *a*-*b* plane. In this paper we report measurements of the anisotropy of three different properties: the field dependence of the Meissner fraction at low fields, hysteresis loops at low temperature, and the temperature dependence of magnetic relaxation.

II. CRYSTAL PREPARATION

The untwinned crystals used in this study were grown in air by a slightly modified version of the Cu-O flux growth procedure described by some of us previously.[9] That paper describes slow-cooling the melted flux to 830 °C and then gradually cooling to room temperature over a period of several more hours. Crystals grown that way generally were orthorhombic, and exhibited (110) twinning even before the postgrowth oxygen anneal. That result indicated that the gradual cooling through the tetragonal-to-orthorhombic transformation temperature (near 650 °C in air[10]) started the conversion. Since the crystals were buried within cavities in the solidified matrix, they were probably under randomly oriented mechanical stress while undergoing the phase transformation. Observations of the mobility of twinning planes under mechanical pressure at these temperatures[11] confirm that randomly oriented mechanical stresses should be able to assist in the formation of twinning planes during the latter segment of the crystal growth temperature cycle. Thus, in later growth attempts we have quenched the crystals to interrupt the slow-cooling segment from a temperature lying between 830 and 865 °C. We did this by pulling the crucibles out of the

furnace. The quenching-in of the tetragonal phase is confirmed by optical microscope observations; isotropic extinction was seen in reflection mode along the c axis with polarizers crossed. The tetragonal crystals were then laid flat on a smooth wafer of polycrystalline $YBa_2Cu_3O_{7-\delta}$ during a postgrowth oxygenation procedure that was used to convert them to orthorhombic crystals having sharp superconducting transitions near 90 K.[12] The crystals were subject to no mechanical stress while being converted from tetragonal to orthorhombic.

All crystals produced this way were viewed under a polarizing microscope, as described in Ref. 12. About 40% of the crystals include untwinned domains larger than 100×100 μm^2 in the a-b plane, about 5% have untwinned domains larger than 300×300 μm^2, and occasionally (about every third or fourth successful growth attempt) we obtain a crystal having an untwinned region approximately 1×1 mm^2. Our typical crystals have a thickness along the c axis of about 25 μm. In some cases, the untwinned regions make up only part of an otherwise heavily twinned crystal. In other cases, a crystal is made up of a few oppositely oriented untwinned domains, separated by an odd number of closely spaced (110) twinning planes. Thus, some crystal cleaving is usually necessary in order to isolate untwinned regions for experiments that cannot be done on just part of the sample.

The samples used in the present study were cleaved from their parent crystals by using a simple apparatus consisting of a pair of razor blades mounted parallel to each other and individually controlled by micromanipulators. The crystals could be viewed under an optical microscope during the cleaving operation. This arrangement provided the necessary rigidity and control of the cleaving position.

Measurements were performed on the three crystals shown in Fig. 1. The pictures were taken in an optical polarizing microscope with white light reflected from (001) faces. The polarizer and analyzer were crossed, and the crystals are shown oriented with the [110] axis along the polarizer direction. In this orientation, the dense twinning so prevalent in most other $YBa_2Cu_3O_{7-\delta}$ crystals shows up as dark, straight striations along $[110/1\bar{1}0]$ directions.[12] The crystals in Fig. 1, however, are seen to be almost completely devoid of such striations. Crystals 1 and 3 each show one striation near the center, but this striation must contain an even number of (110) twinning planes, since optical microscopy shows that the regions on either side of it have the same orientation. Crystal 2 has a small, oppositely oriented domain in one corner. While these three crystals are not perfectly untwinned in the strictest sense, the degree of twinning and the fraction of oppositely oriented domain are so small that they should not affect our measurements significantly.

The axis identifications shown in the pictures are based on the color of the domains viewed in our microscope, as described previously.[12] Since Crystal 1 has an irregular shape in the a-b plane and its crystal axes are not aligned with its edges, its magnetic data are harder to interpret. However, Crystals 2 and 3 have a square a-b geometry, and the a and b axes are aligned with the edges. Thus, to account for demagnetization effects in the analysis, we simply use the demagnetization factors for the inscribed prolate ellipsoid having an axis of revolution parallel to the c axis.[13] The values used are listed in Table 1. Within this approximation the internal field strength H is

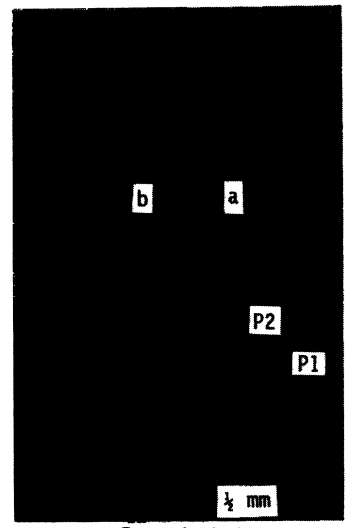

Crystal 1

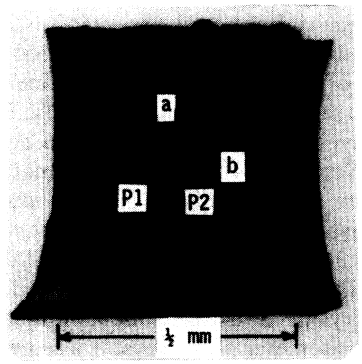

Crystal 2

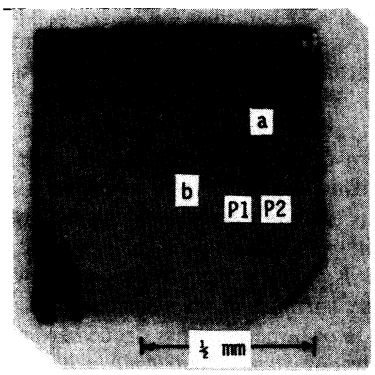

Crystal 3

FIG. 1. Polarized light micrographs of the crystals used. P1 and P2 indicate the polarizer and analyzer directions, respectively, and the a and b axes were identified by an x-ray traceable technique based upon the color contrasts as described in Ref. 12.

TABLE I. Geometrical characteristics of the crystals used. D is the crystal thickness along c and R is the equal-area radius in the a/b plane. N_{ab} and N_c are the calculated demagnetization factors for H perpendicular and parallel to the c axis, respectively.

Crystal	Mass (μg)	D (μm)	R (mm)	N_{ab}	N_c
1	128	22			
2	58	25	0.33	0.03	0.94
3	362	98	0.47	0.07	0.86

uniform, and is the same for an applied field H_a along a and b. This is a much better approximation for Crystals 2 and 3 than for Crystal 1.

III. MEISSNER EFFECT

Each of the three crystals showed a sharp (< 2-K wide) superconducting transition near 90 K in the low field (10 Oe) magnetic susceptibility. The zero-field-cooled susceptibility values are consistently near $-1/4\pi$, indicating full diamagnetic shielding, but the field-cooled values (Meissner fractions) vary for several reasons. Since flux pinning prevents complete expulsion of the magnetic field, the Meissner fraction is expected to vary from crystal to crystal because of sample-dependent differences in the strength of the pinning. The Meissner fraction also depends inversely on the applied magnetic field.[2,6] In addition, we have found that it depends on how quickly the crystal is cooled through the superconducting transition: slower cooling increases the Meissner fraction. Finally, as we shall discuss below, it depends on the orientation of the magnetic field with respect to the crystal.

To probe the a-b anisotropy, we carried out measurements on Crystal 3 using a noncommercial low-field SQUID magnetometer. The crystal was mounted rigidly in a Mylar holder, which was in turn held to a copper insert tip by means of a Mylar flap. Temperature sweeps through T_c at different fields were performed with the crystal in one orientation (H along a). The crystal was then warmed up to room temperature and rotated, and the measurements were repeated in the other orientation (H along b). For each orientation, an initial zero-field-cooled temperature sweep at 10 Oe verified full shielding, and the zero-field-cooled values for each orientation agreed to within 1.4%. The procedure used during the Meissner percent measurements was to cool the sample monotonically at a rate of 1 to 1.5°/min from above 95 K to below 75 K. Data were then taken while warming monotonically through T_c at a similar rate. The reproducibility of data obtained by this procedure was verified.

Typical temperature sweep data are shown in Fig. 2. The a-b anisotropy seen is clearly outside of the scatter. The Meissner fractions found from all of the temperature sweeps on Crystals 1 and 3 are plotted in Fig. 3 as a function of applied magnetic field. The cooling rates were generally much faster and not as carefully controlled for the data of Crystal 1. Nevertheless, we see the same qualitative behavior in both crystals: the Meissner percent is

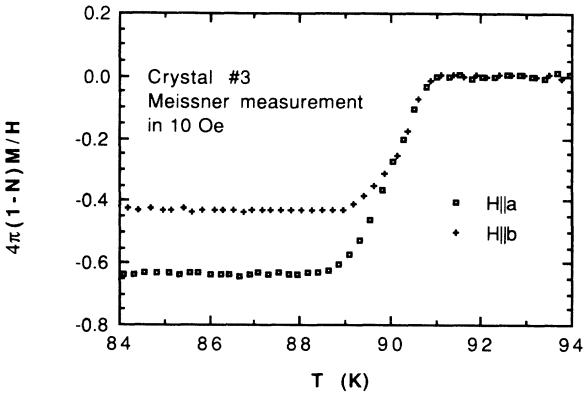

FIG. 2. The field-cooled magnetization for fields oriented along a and b at 10 Oe in Crystal 3.

greater for fields along a than along b in the field range 1–20 Oe.

IV. HYSTERESIS

Measurements of the magnetic hysteresis were performed on the three crystals with the field oriented along each of the three principal axes. The hysteresis loops were measured with a Quantum Design SQUID magnetometer at a fixed temperature of 5 K. Each crystal was

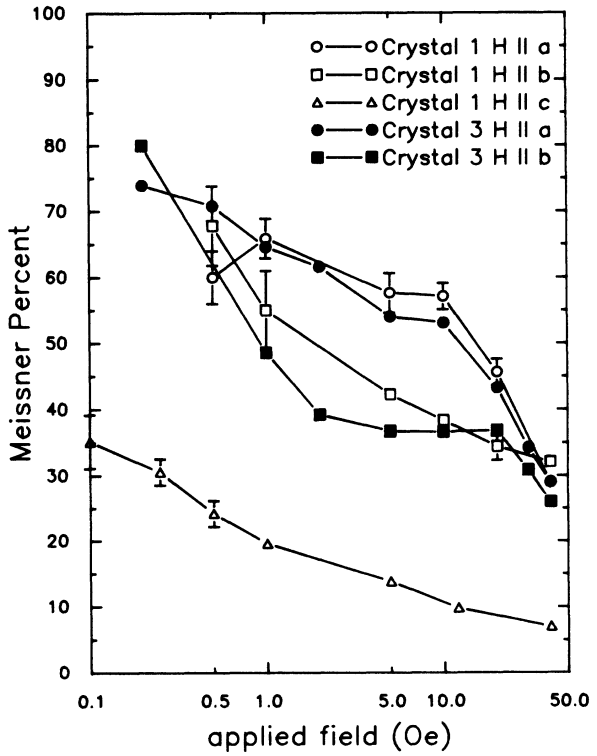

FIG. 3. Field dependence of Meissner percent in Crystals 1 and 3. The lines are guides for the eyes. For clarity, error bars (showing a 90% confidence level) are shown only for the Crystal-1 data. At the lowest fields, there is no anisotropy in the a-b plane, to within the uncertainty of the measurement. The data for Crystal 3 are similar.

mounted in a gelatin capsule with cotton holding it against the inside wall, and this capsule was held rigidly to the sample rod by means of a long plastic straw. A linear fit to the field dependence of the sample holder's magnetic moment was subtracted from the data, but this gave a negligible contribution for fields below 10 kOe. The same sample holder was used for orientation along *a* and *b*. Since magnetic relaxation, to be discussed in Sec. V, is significant, the hysteresis cycles for each crystal orientation were performed at the same rate of 0.09 point/min. A comparison of the data for H along *a* and *b* in Crystal 2 is shown in Fig. 4. The same qualitative behavior was seen in the data for the other two crystals: the hysteresis for fields along *b* was significantly greater than that for fields along *a*.

For completeness, we also show the hysteresis loop on Crystal 3 for H along *c* in Fig. 5. Here no gelatin capsule or cotton was used; the crystal was taped to a flap cut from the straw using Kapton tape. This sample holder gave a negligible moment over the whole field range compared to the larger crystal moment for this orientation. The hysteresis for the field along *c* is much greater than that for the field perpendicular to *c*, as in twinned crystals.[14]

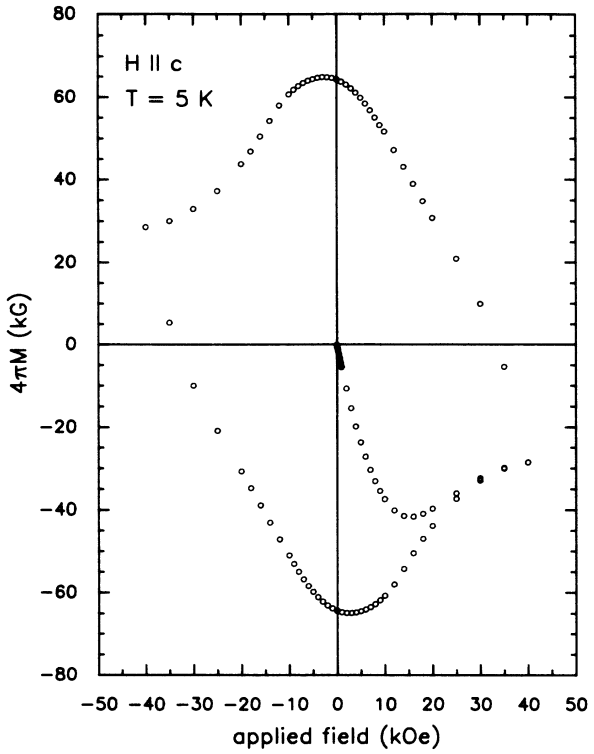

FIG. 5. Hysteresis loop in Crystal 3 at 5 K with H along *c*.

V. MAGNETIC RELAXATION

Measurements of the time decay of the zero-field-cooled magnetic moment were performed on all three crystals, with the applied field along each of the three principal axes. (An S.H.E. SQUID magnetometer was used.) In each case, the crystal was mounted in a gelatin capsule with cotton holding it in place. The capsule was in turn tied rigidly to a long Pyrex rod that was hung from the sample support hook of the magnetometer. Since the ends of the Pyrex rod did not pass through the magnetometer coils while the data were taken, the rod made a negligible contribution to the signal. The moments of the cotton and capsule were also negligible at the 1-kG field used.

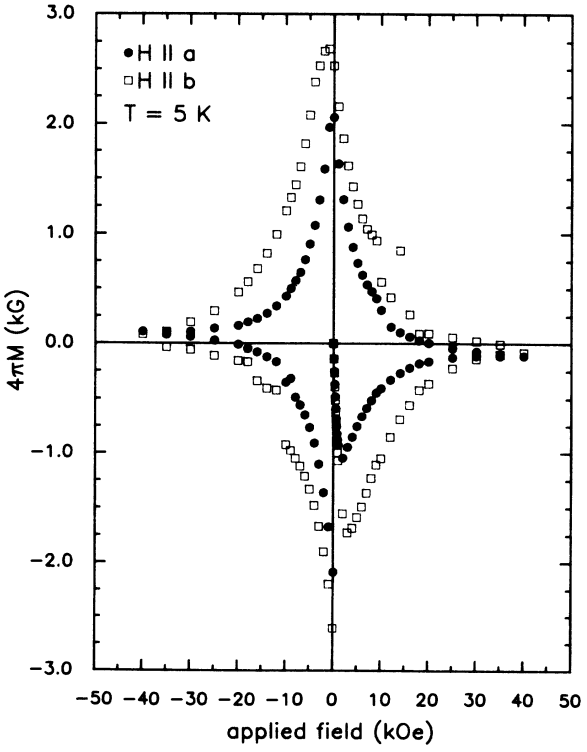

FIG. 4. Hysteresis loops in Crystal 2 for H along *a* and *b*, measured at 5 K, using the same cycle time.

Each relaxation measurement was performed by the following procedure. Before the sample was loaded, the field was set to zero and the temperature was set to the desired value. After the temperature was equilibrated to within 1% of the desired value, the sample was lowered into the cryostat at a speed of 20 mm/min. We have found that such a slow loading in this magnetometer allows the crystal to cool through 90 K before it is exposed to the small remanent field (typically -4 Oe) of the superconducting magnet, thus providing a nearly zero-field cool-down. Also, the temperature was not perturbed noticeably by loading the sample this slowly. A field of 1 kG was then applied in a reproducible way by the computer. After the field was latched and the magnet and shield relaxation effects had subsided, the magnetic moment at constant field and temperature was monitored for about an hour. Finally, the sample was warmed above 90 K by raising it into the room-temperature isolation space, and the whole procedure was repeated at the next temperature.

The data from six typical measurements on crystal 2

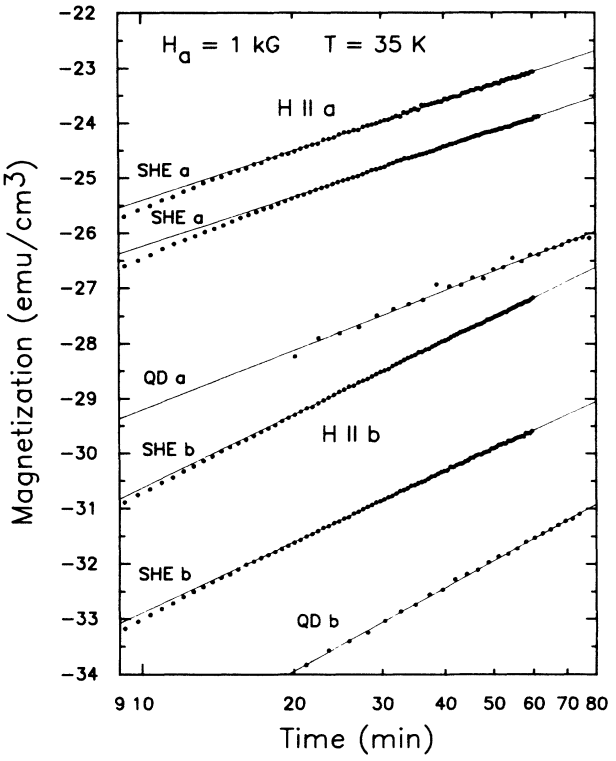

FIG. 6. Time decay of the zero-field-cooled magnetization of Crystal 2 at $T=35$ K and $H_a=1$ kG. The three top data sets are for H along a; the three bottom are for H along b. To show the degree of reproducibility, data sets from two different magnetometers (S.H.E. and Quantum Design) are shown. The solid lines are fits to the data for $t>20$ min.

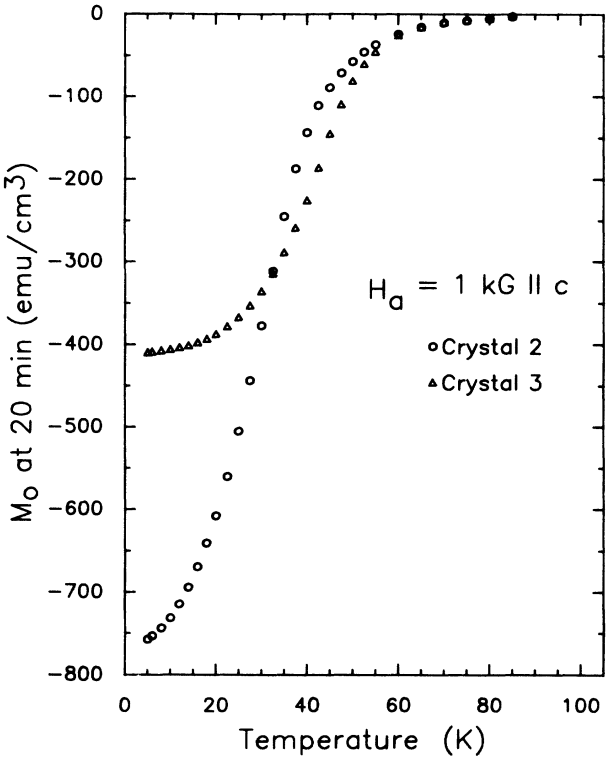

FIG. 7. M_0 vs T for $H_a=1$ kG along c of Crystals 2 and 3.

are plotted in Fig. 6. In agreement with other investigators, we find that the data fit a logarithmic relaxation:

$$M(t)=M_0+S\ln(t/t_0)\ . \tag{1}$$

Figure 6 shows that our data at 35 K deviate from this equation at short times. We find the deviation to be an increasing function of the temperature. Hence, care must be exercised in using Eq. (1), as others have noted (see, e.g., Ref. 15). The three top sets and the three bottom sets of data in Fig. 6 correspond to H along a and b, respectively. All of these data were taken at a temperature of 35 K and an applied field of 1 kG, and the crystal was completely removed from the sample holder between the acquisition of subsequent data sets. Thus, a comparison between the slopes of the top three sets or the bottom three sets gives an idea of the reproducibility of our procedure, and a comparison of the slopes of the top sets with those of the bottom sets indicates the degree of anisotropy of magnetic relaxation at this temperature and field. Both the procedure and the anisotropy were reproducible, even when a different magnetometer (with a different sample mounting scheme) was used.

Our reduction of the data according to Eq. (1), using $t_0=20$ minutes, yields M_0 (M at 20 min) and S ($dM/d\ln t$) as a function of temperature at an applied field of 1 kG. The temperature dependences of M_0 and S with H along c for Crystals 2 and 3 are shown in Figs. 7 and 8. The anisotropy of S between H along a and along b is compared for all three crystals in Figs. 10–12.

VI. ANALYSIS

Let us first consider the temperature derivative (dM_0/dT) of the data of Fig. 7 as shown in Fig. 9. Note that the temperature dependence of dM_0/dT is strikingly similar to S (Fig. 8), though they are by no means equal. Within the experimental uncertainty, the temperatures of the peaks for both quantities are the same for each crystal. This also occurs when the field is applied along the a or b directions, as can be seen by comparing Figs. 11 and 13, and Figs. 12 and 14. This peak temperature, which we denote as T^*, is clearly crystal dependent and orientation dependent. This suggests that the data can be qualitatively understood in terms of flux creep within the critical-state model of Bean,[16] which predicts a crossover in the equations for the temperature dependence of M_0 and S at a temperature which we identify with T^*. The crossover occurs when the flux fronts meet at the center of the sample. For example, for a cylinder of radius R in an axial field H,

$$M_0=\begin{cases}\dfrac{-1}{4\pi}\left[H-\dfrac{10H^2}{4\pi RJ_{c0}}+\dfrac{25H^3}{12\pi^2R^2J_{c0}^2}\right], & T<T^* \\ -RJ_{c0}/30\ , & T>T^*\end{cases} \tag{2a}$$

(2b)

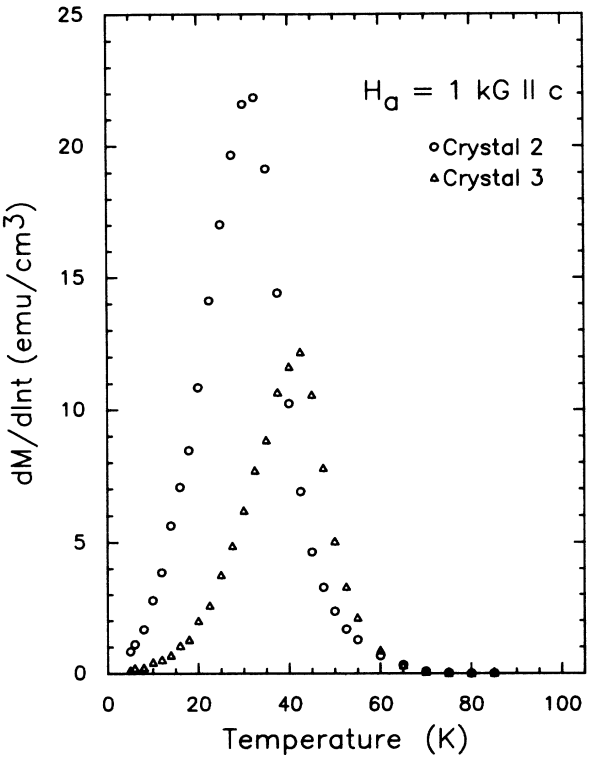

FIG. 8. S vs T for $H_a = 1$ kG along c of Crystals 2 and 3.

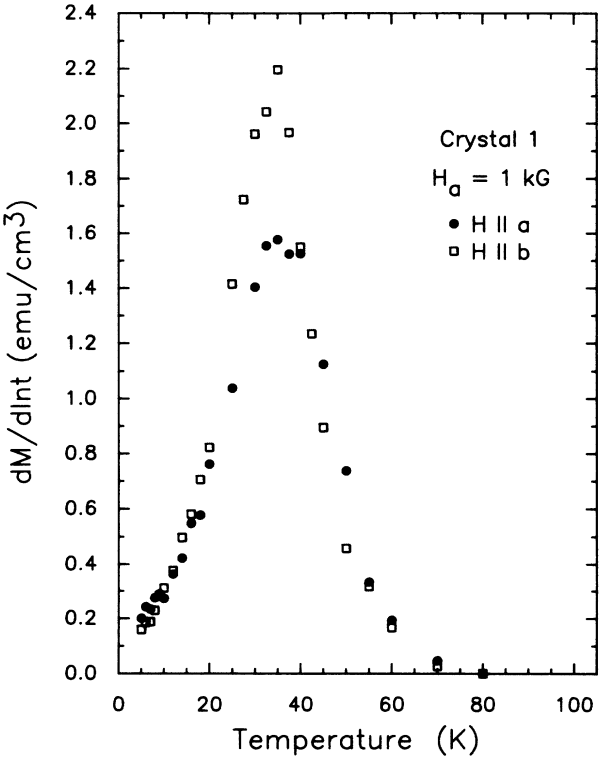

FIG. 10. S vs T of Crystal 1 for $H_a = 1$ kG along a and b.

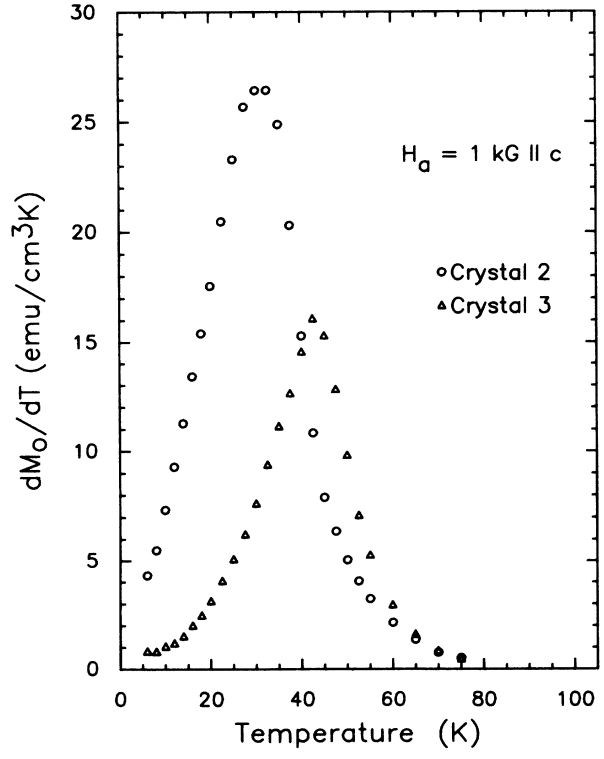

FIG. 9. Derivative of the data of Fig. 7 (dM_0/dT).

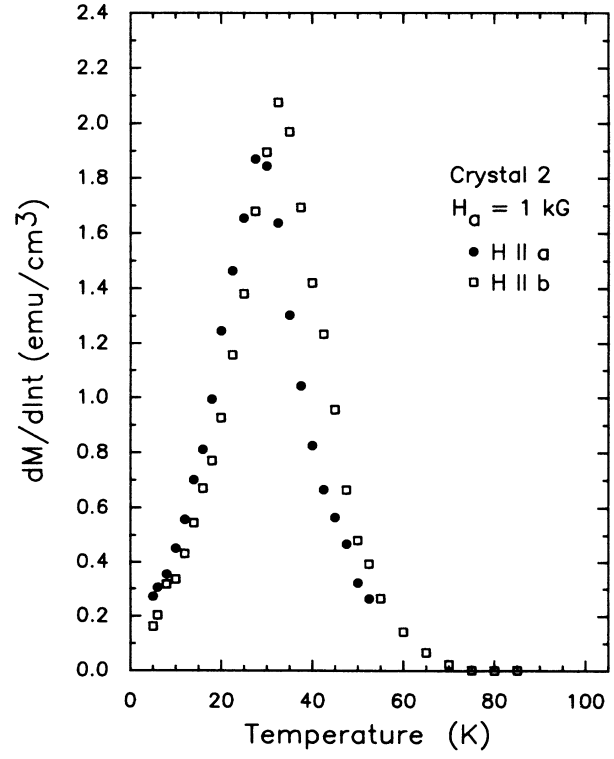

FIG. 11. S vs T of Crystal 2 for $H_a = 1$ kG along a and b.

Here we have simply substituted $4\pi J_{c0}R/10$ for H^* in Bean's results.[16] The temperature dependence of M_0 is implicit in J_{c0}, which falls off sharply with temperature in $YBa_2Cu_3O_{7-\delta}$. Practical units (i.e., Oe, cm, and A/cm^2) are used in these equations and throughout this paper. Physically, H^* and T^* are the minimum field and temperature, respectively, for which flux penetrates the entire sample: T^* is the temperature at which H, the internal field as corrected for demagnetization, equals H^*. J_{c0}, the critical current density in the absence of flux creep, is related to J_c, the measured critical current density, by[17]

$$J_c = J_{c0}[1-(kT/E)\ln(t/\tau)] . \tag{3}$$

Here E is the activation energy for a fluxon hopping over a barrier, assumed for simplicity to be the same throughout the sample, and $1/\tau$ is the characteristic attempt frequency. The measurement time t is 20 min in our measurements. Yeshurun *et al.*[4,5] have analyzed their flux creep data by combining Eq. (3) with the Bean model. In their simplest result,[4] which assumes J_c independent of H and ignores H_{c1}, they find for a cylinder, to lowest order in kT/E,

$$S = \frac{5}{8\pi^2}\left[\frac{H^2}{RJ_{c0}} - \frac{5H^3}{3\pi R^2 J_{c0}^2}\right]\frac{kT}{E}, \quad T < T^* , \tag{4a}$$

$$S = \frac{RJ_{c0}kT}{30E} , \quad T > T^* . \tag{4b}$$

While these equations are expected to fit the data only qualitatively because of the many assumptions, a more involved treatment[5] still predicts a crossover at T^* having

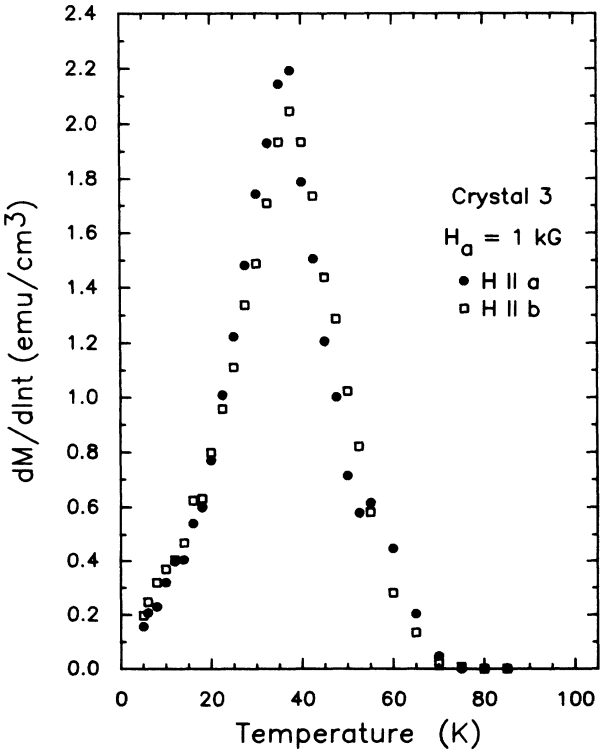

FIG. 12. S vs T of Crystal 3 for $H_a = 1$ kG along a and b.

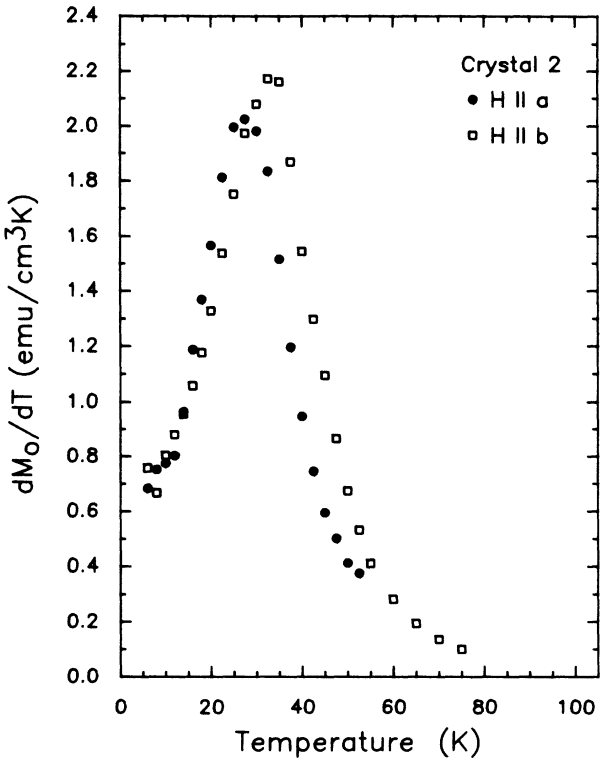

FIG. 13. dM_0/dT vs T of Crystal 2 for $H_a = 1$ kG along a and b.

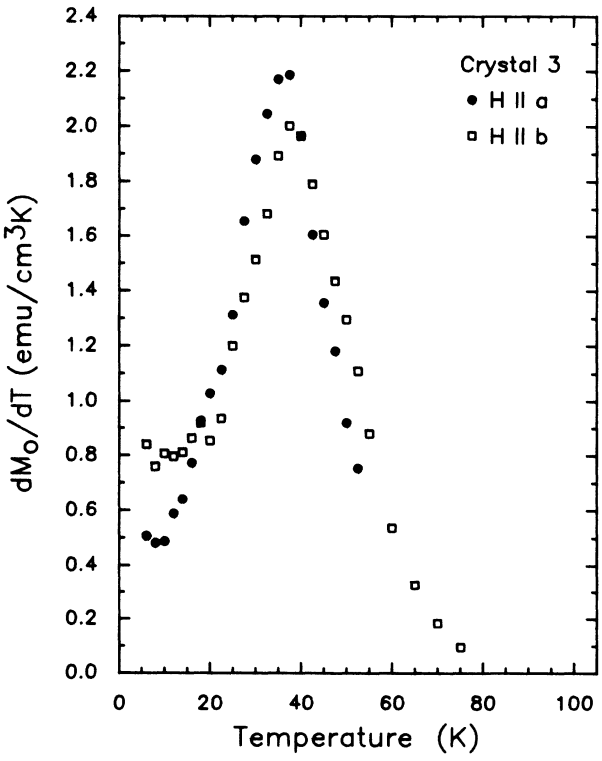

FIG. 14. dM_0/dT vs T of Crystal 3 for $H_a = 1$ kG along a and b.

the same interesting feature: S increases with decreasing J_{c0} below T^*, but decreases with decreasing J_{c0} above T^*. This qualitative behavior holds for the case of a slab as well. (We shall return to this point later.)

We now consider the application of Eq. (2) and (4) to the data of Fig. 7 and 8, respectively. Referring to Table I, we see that the demagnetization factor N_c of Crystal 2 is significantly higher than that of Crystal 3. This accounts for the disparity in the low temperature values of M_0 for these two crystals. The internal field H, given by

$$H = H_a - 4\pi N M_0 , \tag{5}$$

is much higher for Crystal 2 than for Crystal 3 in this orientation, even though the same applied field $H_a = 1000$ Oe was used. Note also that H depends on temperature through $M_0(T)$.

As described above, T^* is the temperature for which H is equal to H^*. Combining the definition of $H^*(T^*)$ with Eq. (5) and Eq. (2b) for $H(T^*)$, we find

$$J_{c0}(T^*) = \frac{5H_a}{2\pi R(1-N/3)} . \tag{6}$$

We can use this to find the qualitative dependence of T^* on crystal dimensions by assuming a qualitatively reasonable temperature dependence for J_{c0}. For example, if we assume[4]

$$J_{c0}(T) = J_{c0}(0)(1-T/T_c)^n , \tag{7}$$

where n is positive, we find

$$T^* = T_c \left[1 - \left[\frac{5H_a}{2\pi(1-N/3)RJ_{c0}(0)} \right]^{1/n} \right] . \tag{8}$$

This shows explicitly that we expect T^* to increase with R and decrease with N for H along c. Referring to Table I, crystal 3 has a higher R and a lower N_c than Crystal 2. Thus Eq. (8) predicts that Crystal 3 will have the higher T^*, just as we find experimentally from the data in Figs. 8 and 9. The analogous equation for T^* when H is along a or b is similar, except of course, we replace R by D, the crystal thickness. Again referring to Table I, Crystal 3 has a higher D than Crystal 2 and the values of N_{ab} are negligible, so we expect Crystal 3 to have the higher T^* for H along a or b. This agrees with our data in Figs. 11–14.

While the anisotropic flux creep data of Figs. 10–14 appear difficult to explain completely, we point out a few common features. Comparing Figs. 13 and 14 (or, alternatively, Figs. 11 and 12), we see that T^* appears to be greater for H along b than for H along a ($T_b^* > T_a^*$) in these, our two best crystals. Referring to Eq. (8), this implies that the critical current density is anisotropic between a and b. For example, if we assume that n is isotropic, we find that $J_{c0}(0)$ is greater for H along b than for H along a. A related feature seen in Figs. 11 and 12 is that S for H along a is generally larger than S for H along b below T_a^*, whereas the inequality reverses above T_b^*. Referring to Eq. (4) and the discussion below it, this implies again that $J_{c0}(T)$ is greater for H along b than for H along a, regardless of whether or not the activation energy E happens to be anisotropic. Further, we note that the hysteresis data of Fig. 4, if interpreted within the Bean model,[16] also indicate that critical currents, responsible for shielding in this case, are larger with H along b than with H along a. Thus, our qualitative interpretation of the a/b anisotropic magnetic relaxation and hysteresis is that the critical current density along a is larger than that along b.

The data for Crystal 1, shown in Fig. 10, are expected to be much more difficult to interpret because of the irregular geometry of that crystal. For example, a small anisotropy in the demagnetizing field would be magnified by the H^3 dependence of S found by Yeshurun *et al.*[5] Even for Crystals 2 and 3, small out-of-plane components of the field due to small crystal-field misalignments would be magnified by the cubic dependence of S on H. We suggest that this is why values of S at T^* do not show a consistent pattern. This is why we have based our interpretations of the S data on features such as T^*, which do not depend so sensitively upon the magnitude of H.

Our measurements of the anisotropic Meissner effect at low fields evidently show that flux pinning is greater for H along b than for H along a. Because the coherence lengths for $YBa_2Cu_3O_{7-\delta}$ are comparable to the lattice constants, it has been suggested that flux pinning could be an intrinsic property of the crystal lattice.[7,8] Perhaps such a model could explain our result. For example, pinning caused by Cu-O chains might be greater when the field is parallel to the chains than when it is perpendicular to them.

VII. CONCLUSIONS

We have developed a method of producing untwinned $YBa_2Cu_3O_{7-\delta}$ single crystals without subjecting them to mechanical stress. From Meissner-effect measurements at low fields, we find that pinning is greater for H along b than for H along a. By combining the results of hysteresis measurements with relaxation measurements analyzed in terms of the standard flux creep model, we find that the critical current density is greater along a than b. If the superconductivity were a property mainly of the Cu-O chains, this would be surprising, but it is known[18–23] that the Cu-O planes dominate the superconducting properties. Our measurements of Meissner effect, hysteresis, and zero-field-cooled relaxation in untwinned crystals are qualitatively similar to those of others in twinned crystals.

ACKNOWLEDGMENTS

We are grateful to T. A. Friedmann, J. Giapintzakis, M. E. Reeves, E. D. Bukowski, and S. E. Stupp for useful conversations. Financial support for this work was provided (for J.P.R., D.M.G., and M.W.R.) by National Science Foundation (NSF) Grant No. DMR 87-14555 and (for K.G.V. and G.W.C.) by the U.S. Department of Energy, Basic Energy Sciences—Material Sciences, under Contract No. W-31-109-ENG-38. One of us (K.G.V.) acknowledges partial support from the Division of Educational Programs, Argonne National Laboratory. Additional funding for this work (for K.G.V., M.W.R., and D.M.G.) was provided by the Science and Technology Center for Superconductivity.

*Also at University of Illinois, Chicago, Chicago, IL 60680.

[1]T. R. Dinger, G. J. Dolan, D. Keane, T. R. McGuire, T. K. Worthington, R. M. Yandrofski, and Y. Yeshurun, in *Proceedings of the 1989 Symposium on High Temperature Superconducting Oxides,* edited by S. H. Whang and A. Das Gupta (Minerals, Metals, and Materials Society, Warrendale, Pennsylvania, 1989).

[2]A. P. Malozemoff, in *Physical Properties of High Temperature Superconductors I,* edited by D. M. Ginsberg (World Scientific, Singapore, 1989).

[3]Y. Yeshurun and A. P. Malozemoff, Phys. Rev. Lett. **60**, 2202 (1988).

[4]Y. Yeshurun, A. P. Malozemoff, and F. Holtzberg, J. Appl. Phys. **64**, 5797 (1988).

[5]Y. Yeshurun, A. P. Malozemoff, F. Holtzberg, and T. R. Dinger, Phys. Rev. B **38**, 11 828 (1988).

[6]L. Krusin-Elbaum, A. P. Malozemoff, Y. Yeshurun, D. C. Cronemeyer, and F. Holtzberg, Physica **153-155C**, 1469 (1988).

[7]M. Tachiki and S. Takahashi, Solid State Commun. **70**, 291 (1989).

[8]G. J. Dolan, G. V. Chandrashekhar, T. R. Dinger, C. Feild, and F. Holtzberg, Phys. Rev. Lett. **62**, 827 (1989).

[9]J. P. Rice, B. G. Pazol, D. M. Ginsberg, T. J. Moran, and M. B. Weissman, J. Low Temp. Phys. **72**, 345 (1988).

[10]J. D. Jorgensen, M. A. Beno, D. G. Hinks, L. Soderholm, K. J. Volin, R. L. Hitterman, J. D. Grace, I. K. Schuller, C. U. Segre, K. Zhang, and M. S. Kleefisch, Phys. Rev. B **36**, 3608 (1987).

[11]J. Giapintzakis, D. M. Ginsberg, and P.-D. Han, J. Low Temp. Phys. **77**, 155 (1989).

[12]J. P. Rice, E. D. Bukowski, and D. M. Ginsberg, J. Low Temp. Phys. **77**, 119 (1989).

[13]H. Zijlstra, *Experimental Methods in Magnetism* (North-Holland, Amsterdam, 1967), pp. 67, 68.

[14]T. R. Dinger, T. K. Worthington, W. J. Gallagher, and R. L. Sandstrom, Phys. Rev. Lett. **58**, 2687 (1987).

[15]C. W. Hagen and R. Griessen, Phys. Rev. Lett. **62**, 2857 (1989).

[16]C. P. Bean, Rev. Mod. Phys. **36**, 31 (1964).

[17]A. M. Campbell and J. E. Evetts, Adv. Phys. **21**, 199 (1972).

[18]J. M. Tarascon, W. R. McKinnon, L. H. Greene, G. W. Hull, and E. M. Vogel, Phys. Rev. B **36**, 226 (1987).

[19]Y. Maeno, T. Tomita, M. Kyogoku, S. Awaji, Y. Aoki, K. Hoshino, A. Minami, and T. Fujita, Nature **328**, 512 (1987).

[20]J. M. Tarascon, P. Barboux, P. F. Miceli, L. H. Greene, G. W. Hull, M. Eibschutz, and S. A. Sunshine, Phys. Rev. B **37**, 7458 (1988).

[21]G. Xiao, M. Z. Cieplak, D. Musser, A. Gavrin, F. H. Streitz, C. L. Chien, J. H. Rhyne, and J. A. Gotaas, Nature **332**, 238 (1988).

[22]Y. Tokura, J. B. Torrance, T. C. Huang, and A. I. Nazzal, Phys. Rev. B **38**, 7156 (1988).

[23]C. H. Pennington and C. P. Slichter, in *Physical Properties of High Temperature Superconductors II,* edited by D. M. Ginsberg (World Scientific, Singapore, 1990), Chap. 5.

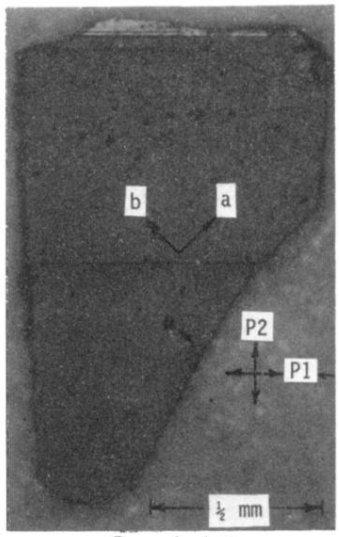

Crystal 1

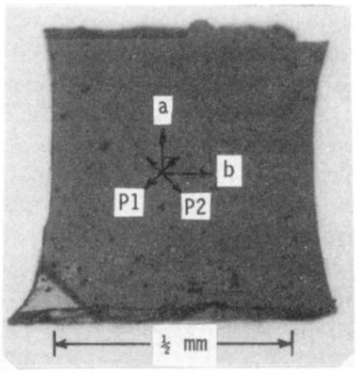

Crystal 2

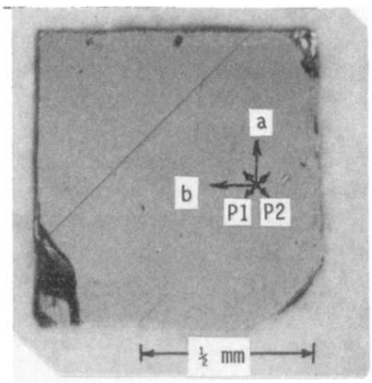

Crystal 3

FIG. 1. Polarized light micrographs of the crystals used. P1 and P2 indicate the polarizer and analyzer directions, respectively, and the *a* and *b* axes were identified by an x-ray traceable technique based upon the color contrasts as described in Ref. 12.